Journal of Environmental Management 219 (2018) 285–293

Contents lists available at ScienceDirect

Journal of Environmental Management

journal homepage: www.elsevier.com/locate/jenvman

Research article

Cetyltrimethylammonium bromide intercalated and branched polyhydroxystyrene functionalized montmorillonite clay to sequester cationic dyes

El-Refaie Kenawy[a], Ayman A. Ghfar[a,b], Saikh Mohammad Wabaidur[b], Moonis Ali Khan[b,*], Masoom Raza Siddiqui[b], Zeid A. Alothman[b], Ayoub Abdullah Alqadami[b], Muhammad Hamid[c]

[a] Department of Chemistry, Polymer Research Group, Faculty of Science, Tanta University, Tanta 31527, Egypt
[b] Chemistry Department, College of Science, King Saud University, Riyadh 11451, Saudi Arabia
[c] Department of Chemical Engineering, Faculty of Engineering, Universitas Malikussaleh, Lhokseumawe-Aceh, Indonesia

ARTICLE INFO

Keywords:
Cetyltrimethylammonium bromide
Montmorillonite
Rhodamine B
Crystal violet
Methylene blue
Intercalation

ABSTRACT

Herein, Cetyltrimethyl ammonium bromide (CTAB) intercalated and branched polyhydroxystyrene (BPS) functionalized montmorillonite (MMT) nano-composite (BPS-CTAB-MMT) was developed, characterized, and its potential as an adsorbent was tested in sequestering cationic dyes viz. rhodamine B (RB), crystal violet (CV), and methylene blue (MB) from aqueous environment. N_2 adsorption/desorption isotherm showed mesoporous BPS-CTAB-MMT surface with a BET surface area of 273.8 m^2/g. The appearance of sharp spikes at 2855 and 2925 cm^{-1} (associated with symmetric and asymmetric tensions of C – H bonds) in infra-red spectrum of BPS-CTAB-MMT indicates successful intercalation of MMT with CTAB and functionalization with BPS. The observed crystallite size of BPS-CTAB-MMT was 66 nm. Comparatively greater weight loss for BPS-CTAB-MMT (11%) than MMT (9%) was observed during thermogravimetric analysis. The adsorption of dyes on BPS-CTAB-MMT was pH dependent with maximum uptake was observed in the pH range: 5–6. For initial dyes concentration (C_o) range: 50–150 mg/L, the observed equilibration time for CV was 300 min, whereas for RB and MB the equilibration time varied between 300 and 360 min. Modeling investigations revealed the applicability of Sips isotherm and pseudo-second-order (PSO) kinetic models to dyes adsorption data. Sips maximum adsorption capacity (q_s) values for RB, CV, and MB at 55 °C were 476.5, 438.7, and 432.7 mg/g, respectively. The adsorption of dyes on BPS-CTAB-MMT was thermodynamically favorable. Desorption studies showed 42.1% RB and 41.9% CV recovery with 0.1 M NaOH and CH_3COCH_3, respectively, while only traces of MB were recovered with tested eluents.

1. Introduction

Dyes and pigments are widely used in textile, paper, plastic, rubber, concrete, paint, and pharmaceutical industries (Yusuf et al., 2017). Among them, textile industry is a major consumer of dyes. About 10% of the dyes used in industries are discharged into the surroundings posing potential environmental threats (Bazin et al., 2012). The dyes dissemination into the water bodies leads to colored water, which is a serious public concern. Also, the dispersed dyes molecules obstruct sunlight from reaching the bulk of the affected water system, leading to the decline in dissolved oxygen level in the polluted water. The presence of dyes may also increase the biochemical oxygen demand of the contaminated water (Ahmad et al., 2015). Dyes are non-biodegradable molecules. Most of the dyes are carcinogenic and often causes allergies like dermatitis, and skin irritation (Yusuf et al., 2015). Due to their lethal impacts on biota, the treatment of dyes-contaminated effluent is essential.

Various treatment techniques and materials like adsorption, biological treatment, oxidation, ion-exchange, filtration, precipitation, electrolysis, reverse osmosis, coagulation, biofloulents, and biodegradable materials have been employed to remove dyes from wastewater. Synthetic dyes, on the other hand cannot be efficiently decolorized by the conventional treatment methods viz. activated sludge process, coagulation, oxidation etc. Among the techniques stated above, adsorption is arguably the most sought after techniques for removing dyes from industrial effluents and wastewater owing to its excellent efficiency, process simplicity as well as cost effectiveness (Forgacs et al., 2004; Khan et al., 2008).

* Corresponding author.
E-mail addresses: mokhan@ksu.edu.sa, moonisalikhan@gmail.com (M.A. Khan).

https://doi.org/10.1016/j.jenvman.2018.04.121
Received 4 January 2018; Received in revised form 8 April 2018; Accepted 30 April 2018

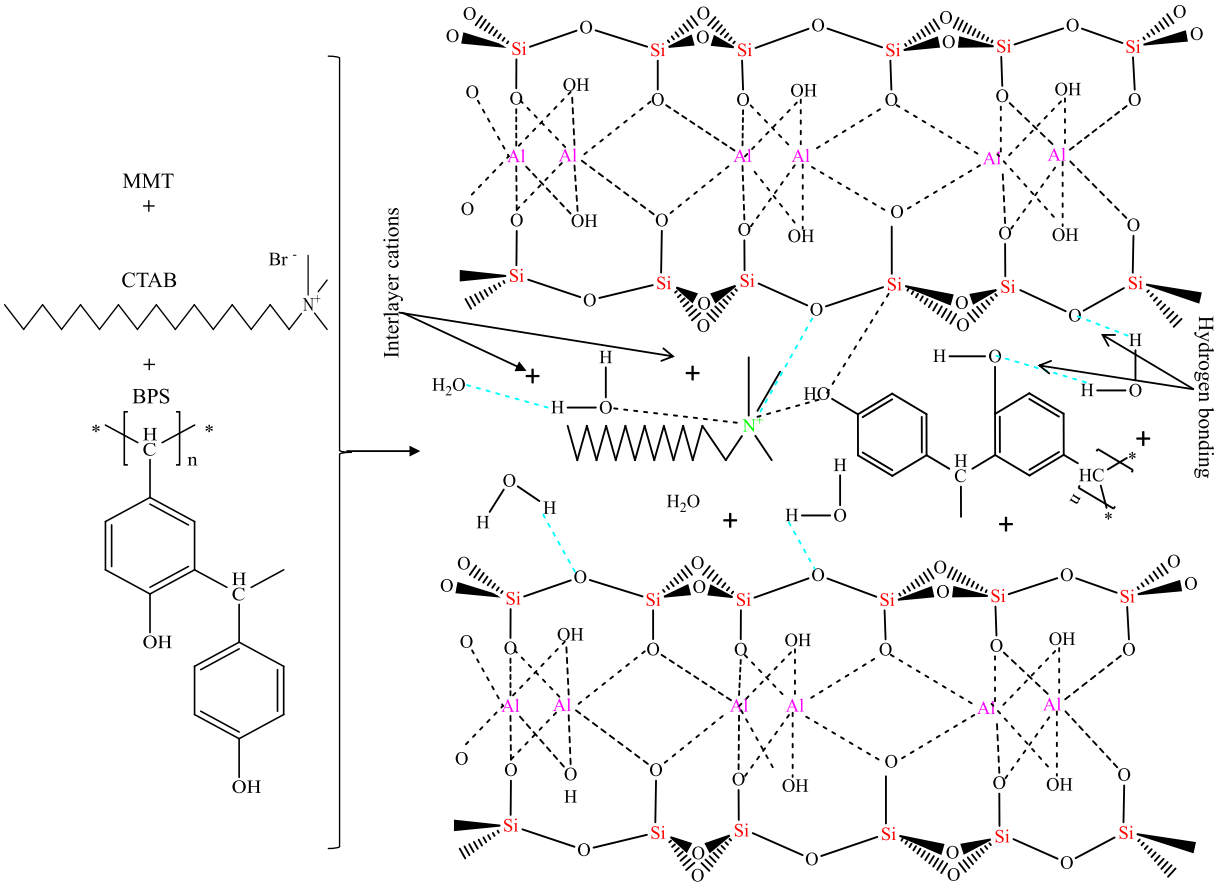

Scheme 1. Intercalation and functionalization of MMT.

During recent years, the use of clay and clay minerals as an adsorbent and heterogeneous catalyst in water remediation operations has increased as they are cost-effect and ecologically safe. Montmorillonite (MMT), a di-octahedral layered cationic clay, classified under 2:1 smectite type clay minerals family, having a molecular formula $M_x(Al_{2-x}Mg_x)(Si_4)O_{10}(OH)_2{\cdot}nH_2O$ (Kumar et al., 2014). Structural arrangement of MMT showed the presence of an octahedral alumina sheet in between two tetrahedral silica sheets forming a layer. The distance between two consecutive aluminosilicate layers in MMT is known as interlayer spacing. The partial isomorphous substitution of ions present in between interlayer spacing of MMT causes charge imbalance. Therefore, to stabilize the charge deficit, hydrated alkali and alkaline earth metal cations occupy the interlayer spacing of MMT. These cations are highly exchangeable and thereby make MMT accommodative for various guest molecules in between its interlayer space.

Previous studies have reported the use of macromolecules such as surfactants in MMT intercalation and its applications in aqueous environment remediation. During intercalation process the interlayer spacing between the nearby MMT layers enlarged, and thus, increasing its surface area resulting in an enhanced sequestering of adsorbate ions. Due to an increase in interlayer gap, the surface energy reduces, resulting in conversion of hydrophilic silicate surface to hydrophobic and therefore, enhancing its adsorption potential (Liu et al., 2011). Wang and Wang (2008) observed a drastic increase in congo red adsorption on CTAB-MMT to 229 mg/g from 10.2 mg/g on MMT. Chen et al. (2011) reported the intercalation of MMT with both cationic (CTMAB) and anionic (SSTA) surfactants and determine its applicability in the removal of methyl orange. CTMAB/10SSTA-MMT showed the highest adsorption capacity for methyl orange. Gemini surfactants intercalated MMT was tested for the removal of methyl orange with an improved adsorption on (18-3-18)-MMT-3 (Liu et al., 2011). A highly effective adsorption of acid red G was observed on octadecyltrimethyl ammonium-MMT (Tong et al., 2010). Dodecyl sulfobetaine surfactant-modified MMT showed an appreciably high adsorption capacity (254 mg/g) for methylene blue (Fan et al., 2014).Though, the previous studies have reported the intercalation of MMT by different surfactants and their applications in removing dyes from aqueous phase but comprehensive literature survey revealed that limited studies are available on functionalization of surfactant intercalated MMT.

In the present study, MMT was intercalated with cethyltrimethyl ammonium bromide (CTAB) to increase the interlayer spacing. Furthermore, to enhance its adsorption potential, CTAB-MMT was functionalized with branched polyhydroxystyrene (BPS). The developed CTAB-BPS-MMT nano-composite was characterized using XRD, FT-IR, DSC, SEM and TEM-EDX, TGA analysis and its application as an adsorbent was tested in the removal of cationic dyes viz., rhodamine B (RB), methylene blue (MB), crystal violet (CV) from aqueous medium. The effects of pH, temperature, initial dyes concentration, and contact time on the adsorption were studied. Isotherm, kinetics, and thermodynamic parameters were evaluated to calculate the dyes adsorption controlling mechanisms on intercalated CTAB-BPS-MMT nano-composite surface.

2. Experimental

2.1. Chemicals and reagents

Montmorillonite K10 (MMT) was procured from Aldrich, Germany. Cethyltrimethyl ammonium bromide (CTAB) was purchased from Sigma, USA. Crystal violet (CV), methylene blue (MB), and rhodamine B (RB) dyes were obtained from Merck and Sigma-Aldrich, Germany, respectively. Branched polyhydroxystyrene (BPS) was procured from

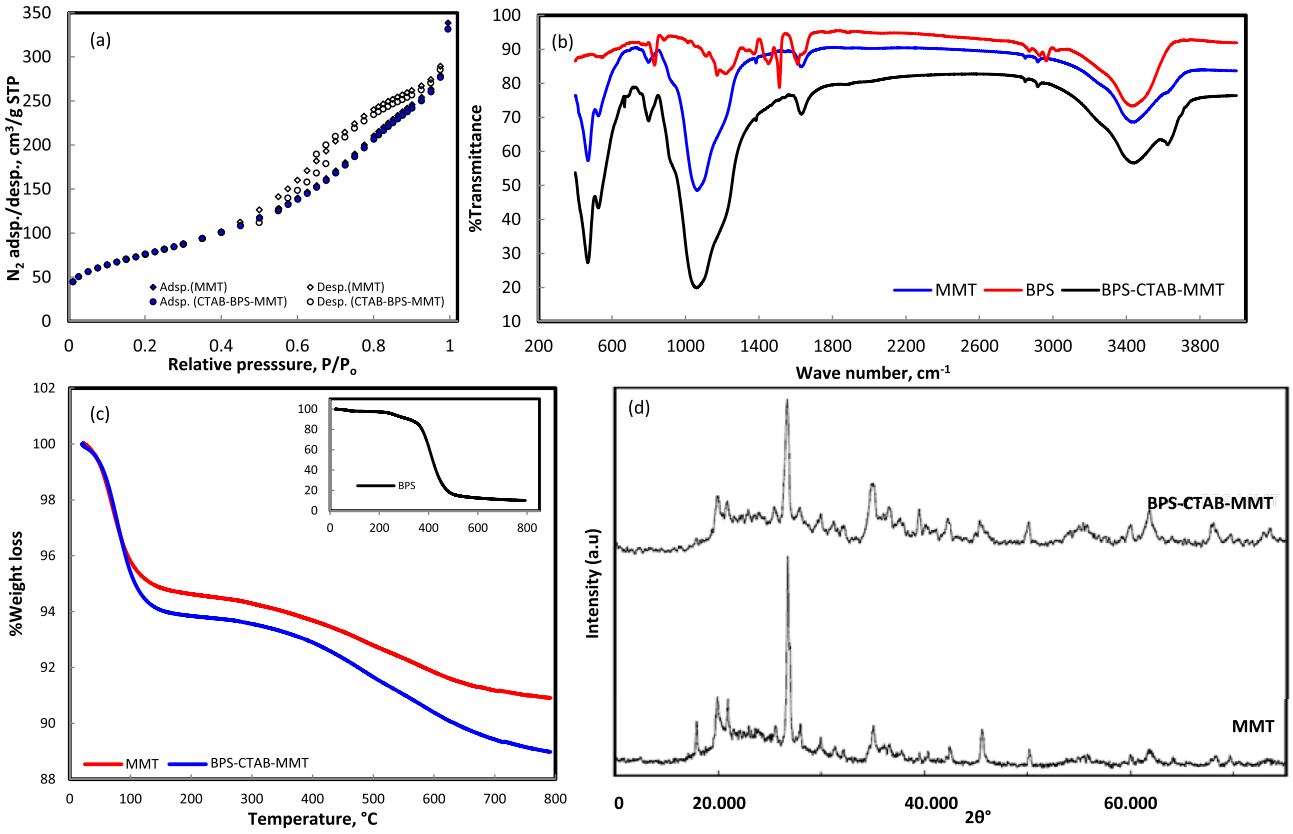

Fig. 1. Adsorption/desorption plot-(a), FT-IR spectrum (b), TGA plots (Inset: BPS) (c), and XRD patterns (d).

Hydrite chemical, USA. Hydrochloric acid (HCl), and nitric acid (HNO_3) were purchased from BDH, UK. Acetic acid (CH_3COOH) was purchased from Qualichem, India. Methanol (CH_3OH) and diethyl ether ($C_2H_5OC_2H_5$) were procured from Fisher Scientific, UK. Ethanol (C_2H_5OH) and acetone (CH_3COCH_3) were purchased from Sigma-Aldrich, Germany and WinLab, UK, respectively. All the chemicals and reagents used in the present research were of analytical reagent (A.R) grade or as itemized.

2.2. Montmorillonite intercalation and functionalization

To intercalate MMT, 50 g of MMT was suspended in 600 mL 1% CTAB solution under continuous stirring at 400 rpm for 24 h. To functionalize CTAB intercalated MMT (CTAB-MMT) surface, 1 gm of BPS was added to the suspension under continuous stirring at 400 rpm for 24 h. Thereafter, the suspension was filtered through Whatman filter paper (No. 1) and was washed multiple times with deionized (DI) water until near to neutral pH was achieved. The BPS functionalized intercalated MMT (BPS-CTAB-MMT) nano-composite was dried at 50 °C under vacuum conditions for 24 h. Scheme 1 systematically demonstrates the synthesis procedure of BPS-CTAB-MMT.

2.3. Characterization of MMT and BPS-CTAB-MMT

The specific surface area of MMT and BPS-CTAB-MMT samples was determined by using Micromeritics–Gemini VII 2390 V1.03 surface area analyzer. The functional groups present on MMT, BPS, and BPS-CTAB-MMT surface were tested through Nicolet 6700 Thermo Scientific Fourier-transform infrared (FT-IR) spectrometer. The thermal stability of MMT, BPS, and BPS-CTAB-MMT was analyzed through Mettler Toledo Thermogravimetric analyzer (TGA)/SDTA851 with Starc software in temperature domain: 25–850 °C, under N_2 flow at 10 °C/min heating scale. X-ray diffraction (XRD) analysis of MMT and BPS-CTAB-MMT was carried out using Philips Xpert X-ray diffractometer. Surface morphology and elemental composition of MMT and BPS-CTAB-MMT were examined on Scanning Electron Microscope (SEM), Hitachi Co. Japan, Model No. S3400N coupled with Energy Dispersive X-ray (EDX), Thermo Scientific Co., USA.

2.4. Batch adsorption and desorption experiments

Twenty five milliliter synthetic dyes (RB, MB, and CV) solutions of desired concentrations were equilibrated with 0.02 g BPS-CTAB-MMT in 100 mL Erlenmeyer flasks over a temperature controlled water bath shaker at 100 rpm. At equilibrium, the solid/solution phases were separated via filtration and residual dyes concentrations were quantitatively determined using a UV–Visible Spectrophotometer (Thermo Scientific Evolution 600, UK) at their respective maximum wave lengths (λ_{max}).

The effect of dye solutions initial pH (pH_i) on their adsorption was analyzed over a pH_i range: 2–10. The solution pH_i was adjusted by adding 0.1 M NaOH/HCl solutions. The effect of initial dyes concentration (C_o: 25–250 mg/L), contact time (t: 0–480 min), and temperature (T: 25–55 °C) on dyes adsorption were also analyzed and optimized. The percentage (%) adsorption and adsorption capacity (q_e) of dye were computed using the equations:

$$\%\text{Adsorption} = \frac{(C_o - C_e)}{C_o} \times 100 \quad (1)$$

$$q_e, \text{ mg/ g} = (C_o - C_e) \times \frac{V}{m} \quad (2)$$

where, C_o and C_e are the initial and equilibrium concentrations of dyes (mg/L) in the solution, respectively. V represents the volume of dyes solution (L) and m is the weight of the BPS-CTAB-MMT (g).

For desorption studies, 0.02 g of BPS-CTAB-MMT samples were saturated with 50 mL dyes solutions of C_o: 50 mg/L in 100 mL Erlenmeyer

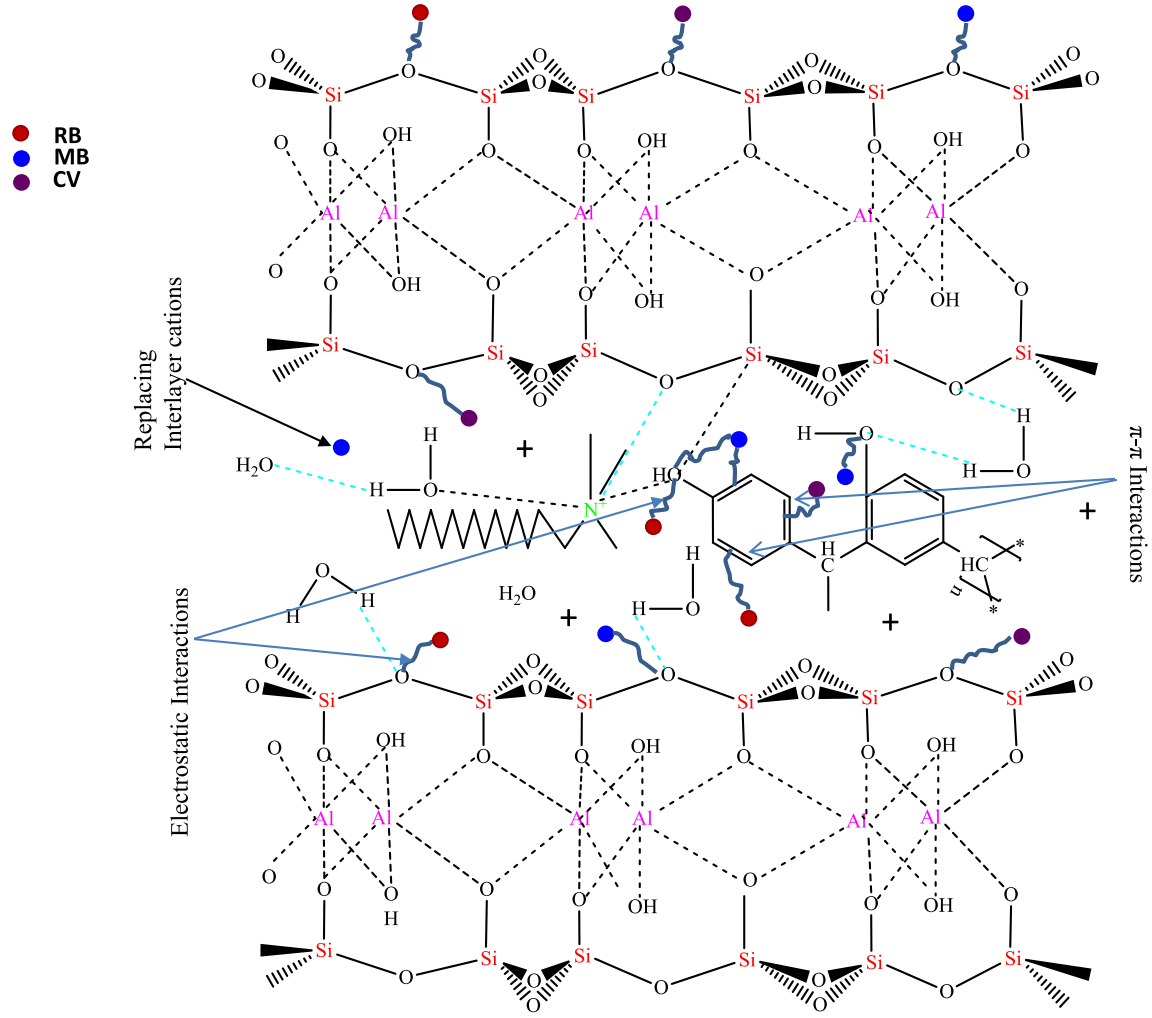

Scheme 2. Proposed mechanism of dyes adsorption on BPS-CTAB-MMT.

flasks. Dyes saturated samples of BPS-CTAB-MMT were separated from aqueous phase through filtration and were washed with D.I water to confirm complete removal of unadsorbed dyes traces. Thereafter, the saturated BPS-CTAB-MMT samples were treated with a series of eluents viz., 0.1 M NaOH, 0.1 M HCl, 0.1 M HNO_3, CH_3COOH, CH_3OH, C_2H_5OH, CH_3OCH_3, $C_2H_5OC_2H_5$ to elute adsorbed dyes. The %desorption of dyes was calculated using the equation.

$$\%\text{Desorption} = \frac{\textit{Concentration of dye ions desorbed by eluent}}{\textit{Initial concentration of dye ions adsorbed on BPS} - \textit{CTAB} - \textit{MMT}} \times 100 \quad (3)$$

3. Results and discussion

3.1. Characterization of BPS-CTAB-MMTand dyes adsorption mechanism

Fig. 1a illustrates type IV adsorption-desorption isotherms with an appearance of hysteresis loops in the P/Po range: 0.40–0.95 for both MMT and BPS-CTAB-MMT, indicating the presence of mesopores on both MMT and BPS-CTAB-MMT surfaces. The observed BET surface area for BPS-CTAB-MMT was 273.8 m^2/g, slightly lower than MMT (274.4 m^2/g), attributed to the blockage of pores present in between interlayer spacing of MMT during its intercalation with CTAB and functionalization with BPS. A gradual decrease in total pore volume from 0.4271 (for MMT) to 0.3924 (for BPS-CTAB-MMT) cm^3/g, while an increase in total pore area from 134.5 (for MMT) to 135.8 (for BPS-CTAB-MMT) m^2/g was observed, agreeing well with previously reported results on MMT intercalation with trimeric surfactant (Liang and Li, 2017).

The FT-IR spectrum of MMT showed bands at 461 and 510 cm^{-1} associated with the Si-O-Mg and Si-O-Al bending frequencies, while a band at 1040 cm^{-1} associated with characteristic Si-O stretching vibrations (Silva et al., 2012; Hassanien et al., 2010) (Fig. 1b). A peak at 800 cm^{-1} was due to the presence of amorphous silica in MMT. A peak at 1610 cm^{-1} was associated with H – O – H deformation (Wang and Zhang, 2011). A broad peak in between 3330 and 3580 $cm^{-1}$was ascribed to –OH group stretching vibrations on MMT (Wang and Wang, 2008). Two weak peaks at 2855 and 2925 cm^{-1}due to the symmetric and asymmetric tensions of C-H bonds were observed on MMT spectrum. These two peaks were more pronounced in BPS and BPS-CTAB-MMT spectra (Fig. 1b), confirming the presence of long branched hydrocarbon chains on BPS and an attachment of hydrocarbon chain with MMT surface during intercalation with CTAB and functionalization with BPS. The bands at 1598 and 1453 cm^{-1} (characteristic bands of polystyrene) on BPS spectrum were attributed to aromatic C=C stretching (Kaniappan and Latha, 2011). The FT-IR spectrum of BPS-CTAB-MMT nano-composite showed a typical band at 3622 cm^{-1} representing smectite group that contains large quantity of Al in the octahedral sheet, attributed to –OH group stretching. A high intensity absorption peak at 3452 cm^{-1}in BPS-CTAB-MMT composite spectrum was associated with –OH group stretching vibrations (Wang and Wang,

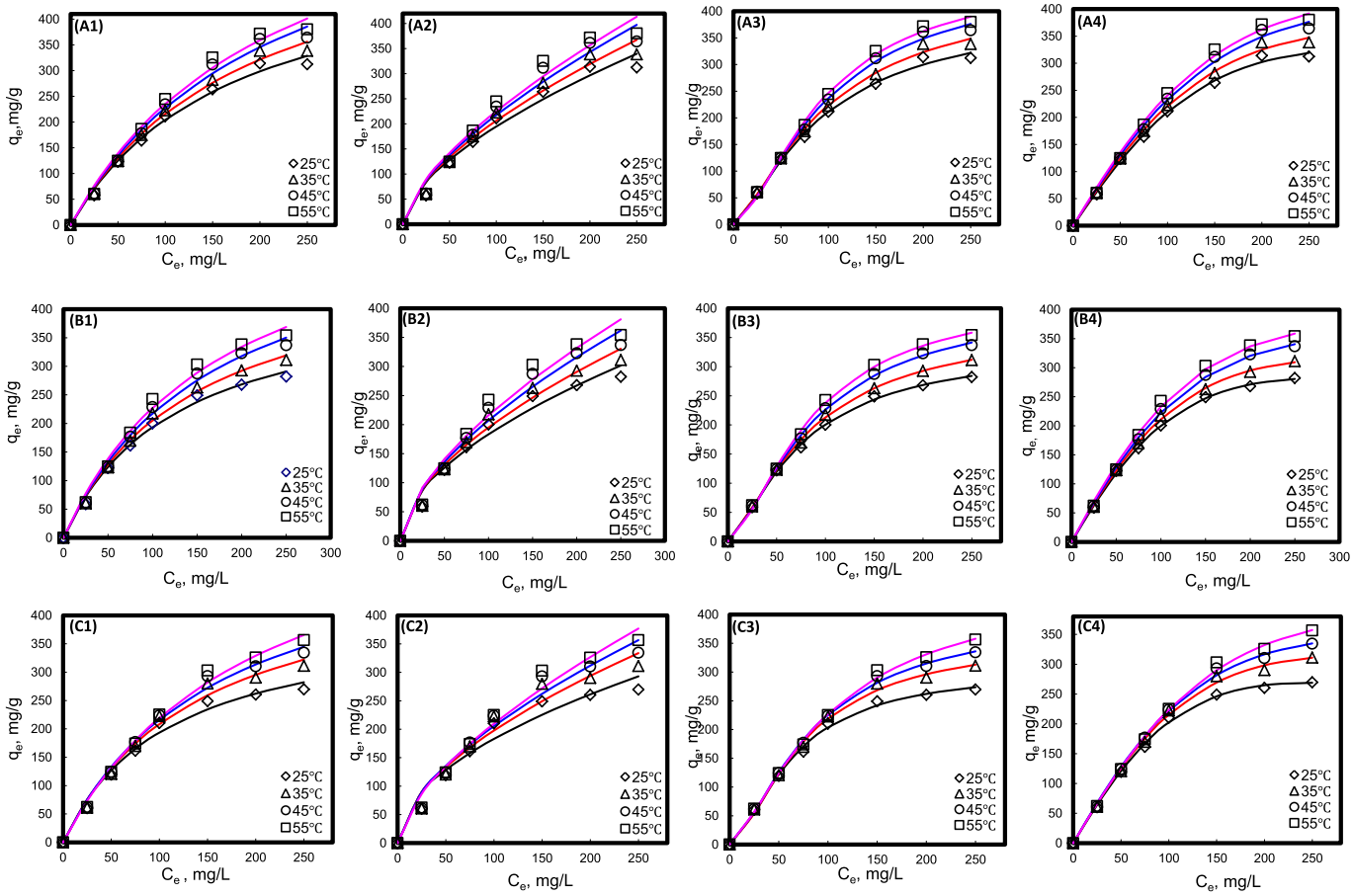

Fig. 2. Langmuir (A1), Freundlich (A2), Sips (A3), Radke-Prausnitz (A4) isotherm models for the adsorption of RB; Langmuir (B1), Freundlich (B2), Sips (B3), Radke-Prausnitz (B4) isotherm models for the adsorption of CV; Langmuir (C1), Freundlich (C2), Sips (C3), Radke-Prausnitz (C4) isotherm models for the adsorption of MB on BPS-CTAB-MMT.

2008).The absorption band at 1610 cm^{-1} in MMT spectrum moved to 1638 cm^{-1} in BPS-CTAB-MMT composite spectrum indicating an increase in hydrophobicity. This also corroborates with successful intercalation of MMT with cationic surfactant (hydrophilic) into the interlayer spacing (Xue et al., 2007). Additionally, the peak intensity of absorption band at 1638 cm^{-1} increases owing to an enhancement in water molecules content due to the swelling effect (a clay surface property).The bands due to Si – O stretching on BPS-CTAB-MMT shifted to comparatively higher wavenumber (1065 cm^{-1}) and its intensity increases remarkably compared to MMT. Also, the spectral bands at 470 and 531 cm^{-1} showed a remarkable gain in their respective intensities compared to MMT. All these spectral changes confirmed successful intercalation and functionalization of MMT.

Fig. 1c elucidates the TGA plots of MMT and BPS-CTAB-MMT. The total weight loss of 9 and 11% in two stages were observed for MMT and BPS-CTAB-MMT samples, respectively. During first stage, ranged between 25 and 150 °C, 5 and 6% weight loss due to the loss of physisorbed water molecules were observed for both MMT and BPS-CTAB-MMT, respectively. During the second stage, ranged between 150 and 725 °C, 4 and 5% weight loss was observed for both MMT and BPS-CTAB-MMT, respectively. A second stage weight loss was attributed to the loss of hydrated ions present between the interlayer spacing of MMT and BPS-CTAB-MMT samples in temperature range: 150–350 °C. The loss of hydroxyl group from MMT took place in temperature range: 400–600 °C, while a weight loss of BPS-CTAB-MMT above 420 °C was associated with degradation of CTAB chain from interlayer spacing and other organic moieties including BPS (Xue et al., 2007). Additionally, the loss of hydroxyl group from BPS-CTAB-MMT starts at 510 °C. The TGA profile of MMT also confirms that BPS-CTAB-MMT has faced more water loss (1%, w/w) compared to MMT (Tangaraj et al., 2017).

Fig. 1d displayed the XRD patterns of MMT and BPS-CTAB-MMT. The MMT has 2:1 layered structure of smectite class depicted by a sharp peak at 2θ = 26.680 indicating the existence of quartz mineral (Sarma et al., 2016), while peaks at 2θ = 19.860 and 27.950 confirms the presence of beidellite in MMT (Santoso et al., 2017). Here, it is noteworthy to state that a peak at 2θ = 17.870 corresponding to basal spacing (d) – 0.49595 nm, could not be noticed in BPS-CTAB-MMT pattern, might be due to the deformities and changes occurred in the crystallite structure of MMT during the intercalation and functionalization. A peak at 2θ = 26.680 in XRD pattern of MMT corresponding to d – 0.33385 nm changed to 2θ = 26.660 (d – 0.33409 nm) in BPS-CTAB-MMT pattern indicating the insertion of surfactant chains between the layers of MMT clay (Siboni et al., 2015). Additionally, the calculated mean crystallite sizes of MMT and BPS-CTAB-MMT using Scherrer equation were 80 and 66 nm, respectively.

The morphological images of MMT and BPS-CTAB-MMT are shown in Fig. S1. Particles of non-uniform shapes and irregular sizes with fluffy look were observed on MMT surface (Sarma et al., 2016). Fig. S1b demonstrates an appearance of enormous number small particles (along some comparatively bigger particles) on BPS-CTAB-MMT surface due to the intercalation of MMT with CTAB. Also, particles with sharp edges synonymous with rod and crystal shape (Fig. S1a, Inset) appeared on BPS-CTAB-MMT due to the functionalization of CTAB intercalated MMT with BPS. The observed increase in carbon and bromine content on BPS-CTAB-MMT compared to MMT during the elemental analysis implying successful formation of BPS-CTAB-MMT (Figs. S1a and b, Inset).

The MMT surface is negatively charged, therefore, it can bind cationic dyes through electrostatic interactions. However, in between the

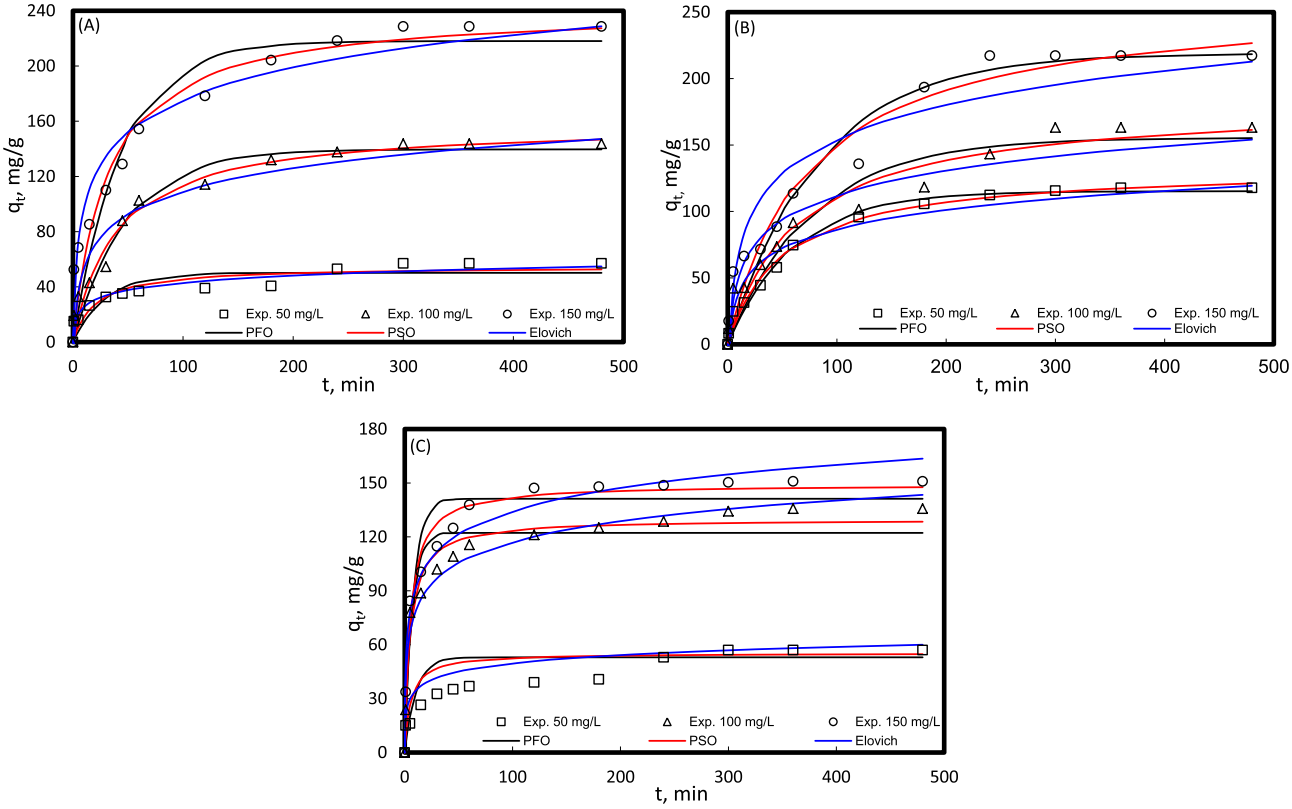

Fig. 3. Kinetic models for CV (A), RB (B), and MB (C) adsorption on BPS-CTAB-MMT.

Table 1
Isotherm data for adsorption of dyes on CTAB-BPS-MMT at varied temperatures.

Isotherm model	CV				MB				RB			
	25 °C	35 °C	45 °C	55 °C	25 °C	35 °C	45 °C	55 °C	25 °C	35 °C	45 °C	55 °C
Langmuir												
K_L, mg/g	3.449	3.441	3.434	3.539	3.687	3.527	3.458	3.284	3.233	3.288	3.323	3.414
a_L, L/g	0.008	0.007	0.0058	0.0056	0.009	0.007	0.006	0.005	0.006	0.005	0.005	0.004
R^2	0.998	0.990	0.987	0.9084	0.972	0.977	0.985	0.989	0.985	0.986	0.982	0.981
R_L	0.0011	0.0012	0.0012	0.0011	0.0011	0.0011	0.0011	0.0012	0.0012	0.0012	0.0012	0.0012
Freundlich												
K_F,(mg/g)(L/g)$^{1/n}$	144.52	94.23	63.15	59.58	252.86	103.35	69.73	42.30	59.09	47.24	36.05	34.88
n	0.544	0.576	0.609	0.618	0.514	0.572	0.602	0.640	0.607	0.630	0.657	0.664
R^2	0.950	0.948	0.958	0.953	0.919	0.938	0.954	0.966	0.958	0.961	0.957	0.955
Sips												
q_s, mg/g	337.75	378.84	417.19	438.67	306.07	362.26	406.39	432.69	406.23	446.31	471.41	476.47
K_s, L/g	0.002	0.002	0.001	0.001	0.001	0.001	0.001	0.002	0.002	0.002	0.001	0.001
m_s	1.408	1.407	1.459	1.537	1.585	1.557	1.473	1.386	1.378	1.389	1.491	1.568
R^2	0.998	0.999	0.999	0.998	0.999	0.998	0.997	0.999	0.994	0.994	0.994	0.996
Radke-Prausnitz												
A, mg/g	15513.1	15011.7	14970.3	14861.2	22054.09	18000.0	16055.8	16000.0	24646.6	20000.5	19000.2	18000.5
B, L/mg	0.00017	0.00018	0.00019	0.00019	0.00012	0.00015	0.00017	0.00017	0.00010	0.00013	0.00015	0.00016
m	1.623	1.591	1.563	1.551	1.703	1.625	1.581	1.554	1.661	1.602	1.570	1.552
R^2	0.990	0.998	0.998	0.995	0.991	0.994	0.996	0.996	0.995	0.995	0.993	0.993

interlayer spacing on MMT surface the presence of exchangeable cations resist the adsorption of the cationic dyes. The intercalation of MMT with CTAB and functionalization with BPS results in an increase in cationic dyes viz. RB, CV, and MB adsorption. This increase in dyes adsorption can be ascribed to the interaction between dyes molecule and hydroxyl group of BPS and was not only limited to the binding through surficial functional groups of MMT. As depicted in Scheme 1 CTAB was firmly attached in between the interlayer spacing of MMT clay both through electrostatic attraction with the negative surface charge and hydrogen bonding with water molecule resulting in an increase in the interlayer space. The attachment of BPS inside the interlayer spacing of MMT was through hydrogen bonding as well as electrostatic interaction between hydroxyl oxygen of BPS and surface Si of MMT and positively charged CTAB. Thus, the cationic dye molecules have more possibilities to be trapped inside the interlayer space through ion-exchange and electrostatic interaction with the negatively charged surface and with BPS thorough π – π interactions between aromatic rings present on BPS and dyes (Scheme 2).

Table 2
Kinetic data for adsorption of dyes on CTAB-BPS-MMT at varied concentrations.

Kinetic model	CV			MB		
	50 mg/L	100 mg/L	150 mg/L	50 mg/L	100 mg/L	150 mg/L
$q_{e,\ exp}$, mg/g	57.00	143.67	228.62	55.90	135.70	150.90
PFO						
$q_{e1,cal}$, mg/g	50.17	139.61	218.07	52.98	122.22	141.22
k_1, 1/min	0.033	0.020	0.023	0.096	0.146	0.127
R^2	0.835	0.966	0.923	0.985	0.979	0.984
PSO						
$q_{e2,cal}$, g/mg-min	56.89	144.71	230.27	55.35	134.80	149.23
k_2	0.0009	0.0002	0.0001	0.0033	0.0015	0.0013
R^2	0.980	0.974	0.944	0.996	0.999	0.999
Elovich						
α, g/mg-min	21.52	22.04	58.94	119.80	181.36	249.73
β, g/mg	0.132	0.041	0.029	0.151	0.059	0.053
R^2	0.911	0.972	0.930	0.995	0.980	0.997

3.2. Adsorption studies

3.2.1. Effect of pH

Fig. S2 demonstrates the adsorption of dyes (RB, MB, and CV) on BPS-CTAB-MMT for pH_i range: 2–10. The adsorption of RB at pH_i: 1.92 was 111.5 mg/g, gradually increases, attaining the maximum observed value (125.3 mg/g) at pH_i: 5. Further increase in RB solution pH_i causes a decline in RB adsorption reaching to minimum (93.3 mg/g) adsorption at pH_i: 10. The adsorption of CV on BPS-CTAB-MMT at pH_i: 3.18 was 106 mg/g, gradually increased to 120.8 mg/g (maximum) at pH_i: 5.75. An insignificant change in CV adsorption with further increase in pH_i was observed. For MB, the adsorption on BPS-CTAB-MMT at pH_i: 2.11 was 84.8 mg/g, gradually increased to a maximum value of 117.6 mg/g at pH_i: 6.15. Further rise in pH_i causes a slight decline in MB adsorption. The aforesaid results showed maximum cationic dyes uptake in pH_i range: 5–6. At lower pH_i, there is a competition between H^+ ions and dyes cations to occupy BPS-CTAB-MMT surface, hence restricting dyes adsorption. As pH_i increases, the concentration of H^+ ions decreases and consequently the adsorption of dyes increases. Moreover, the adsorption of RB was comparatively higher than CV and MB. The higher concentration of oxygen containing functionalities along with nitrogen containing functionalities might be a probable reason for it.

3.2.2. Effect of concentration

The adsorption of dyes at varied initial concentrations (C_o: 25–250 mg/L) on BPS-CTAB-MMT was studied at different temperatures (T: 25–55 °C) (Fig. 2). In general, a proportional increase in dyes adsorption capacities with an increase in concentration and temperature was observed. At 25 °C, for aforesaid concentration range the adsorption capacities of RB, CV, and MB were 57.7–312 mg/g; 58.9–282.1 mg/g; and 60.2–269.6 mg/g, respectively. At 35 °C, for aforementioned concentration range the adsorption capacities of RB, CV, and MB were 57.7–312.4 mg/g; 60.2–311.1 mg/g; and 60.7–311.1 mg/g, respectively. At 45 °C, for aforesaid concentration range the adsorption capacities of RB, CV, and MB were 60.2–338.5 mg/g; 61.2–336.9 mg/g; and 61.2–334.3 mg/g, respectively. At 55 °C, for aforesaid concentration range the adsorption capacities of RB, CV, and MB were 60.4–380.1 mg/g; 62.2–354 mg/g; and 62.1–356.5 mg/g. The increase in RB, CV, and MB adsorption on BPS-CTAB-MMT with increase in concentration was attributed to an increase in collision efficiency between the cationic dye ions and BPS-CTAB-MMT with increase in dyes concentration (Khan et al., 2017). Also, an increase in dyes adsorption with rise in temperature exhibits an endothermic nature of adsorption.

3.2.3. Effect of contact time

The adsorption of RB, CV, and MB on BPS-CTAB-MMT as a function of contact time at varied initial concentrations (C_o: 50–150 mg/L) was studied (Fig. 3). The respective adsorption capacities of CV at C_o: 50, 100, and 150 mg/L were 57, 143.7, and 228.6 mg/g, attaining equilibrium in 300 min at each concentration. For RB, the equilibrium adsorption capacities for aforesaid concentration range were 117.7, 163.2, and 217.2 mg/g, while the equilibration time was ranged

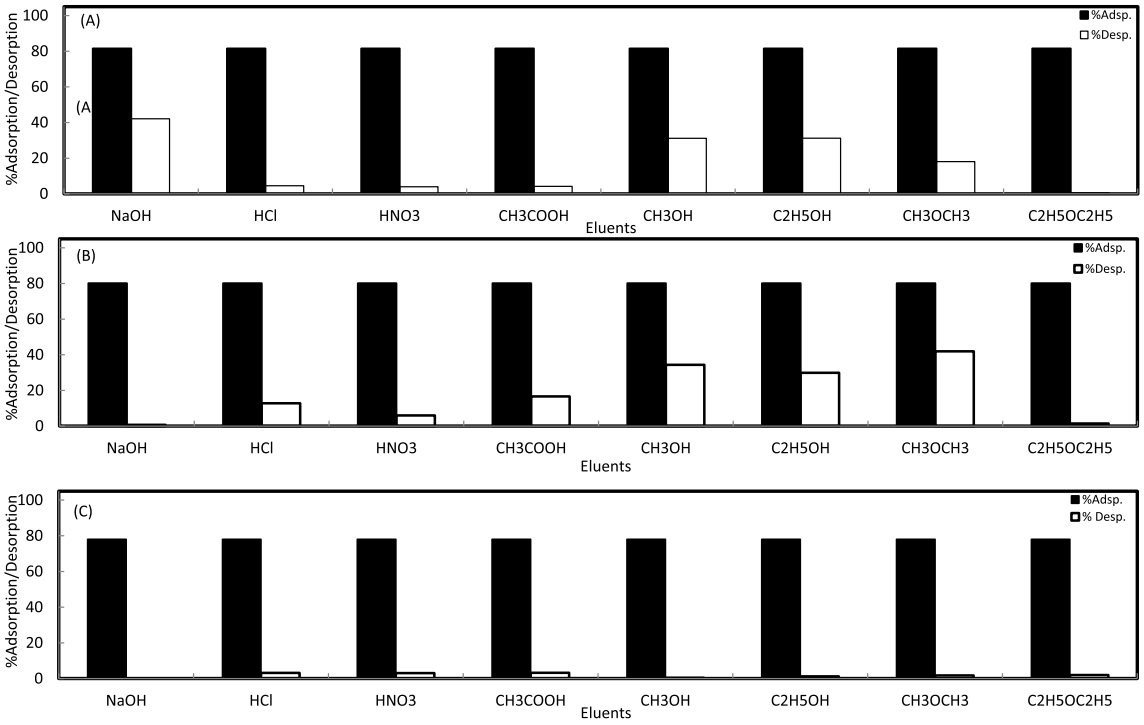

Fig. 4. Desorption plots of RB (A), CV (B), and MB (C) from BPS-CTAB-MMT.

between 300 and 360 min. The observed equilibrium adsorption capacities of MB for aforementioned concentration range were 57, 135.7, 150.9 mg/g, while the equilibration time was ranged between 300 and 360 min.

4. Adsorption modeling

4.1. Isotherm modeling

The adsorption isotherms represent a definite connection among the adsorbate concentration and its degree of adsorption onto the surface of adsorbent at varied temperatures. Langmuir, Freundlich, Sips, and Radke-Prausnitz isotherm models in non-linearized forms were used to quantify the adsorption potential of BPS-CTAB-MMT for different cationic dyes viz., RB, MB, and CV from aqueous solution. The precise information of these models is provided in Supplementary Information (Text S1). Table 1 and Fig. 2 showed the isotherm data and dyes adsorption plots on BPS-CTAB-MMT, respectively. The RB, CV, and MB adsorption data at varied temperatures on BPS-CTAB-MMT was fitted to Sips isotherm model, as depicted by higher correlation coefficient (R^2) values and isotherm plots in Fig. 2A3, B3 and C3. Hence, it could be concluded that adsorption of RB, CV, and MB on BPS-CTAB-MMT at lower adsorbate concentrations is heterogeneous adsorption characterizing Freundlich isotherm, while at higher adsorbate concentrations it showed monolayer adsorption characteristic of Langmuir isotherm model as Sips isotherm model is a hybrid form of both Langmuir and Freundlich isotherm models. The magnitudes of separation factor (R_L) for the adsorption of RB, CV, and MB on BPS-CTAB-MMT at varied temperatures were in between 0.0011 and 0.0012 suggesting favorable adsorption process. The maximum adsorption capacities (q_s) calculated by Sips isotherm model for RB, CV and MB in temperature range: 25–55 °C were 406.2–476.5 mg/g; 337.7–438.7 mg/g; 306.1–432.7 mg/g, respectively.

4.2. Kinetic modeling

The kinetic modeling describes uptake rate of solute and clearly these rate governs the residence time of adsorbate uptake at the solid-liquid interface including the diffusion process. During the study RB, CV, and MB adsorption data at varied concentrations was modeled by pseudo-first-order (PFO), pseudo-second-order (PSO), and Elovich equation. The detailed information regarding these models is provided in Supplementary Information (Text S2). Table 2 and Fig. 3 illustrate kinetic modeling data and plots, respectively. Results showed better fitting of RB, CV, and MB adsorption kinetic data at varied concentrations to PSO model as depicted by higher R^2 values and kinetic plots fittings. Moreover, the nearer $q_{e,\ exp}$and $q_{e2,\ cal}$ also supported the applicability of PSO model to the data.

4.3. Thermodynamic parameters

The thermodynamic parameters viz. standard enthalpy change (ΔH°), standard entropy change (ΔS°), and Gibb's free energy change (ΔG°) for the adsorption of RB, CV, and MB on BPS-CTAB-MMT were evaluated. The comprehensive material about these parameters is presented in Supplementary Information section (Text S3). The negative values of ΔG° at varied temperatures for RB, CV, and MB indicated the feasibility of adsorption process (Table S1). A decline in ΔG° magnitude with temperature showed a rise in process spontaneity. The positive ΔH° values indicated endothermic nature of dyes adsorption on BPS-CTAB-MMT. The ΔH° magnitude for CV was maximum (12.79 kJ/mol) among the studied dyes showing comparatively stronger interaction between CV and BPS-CTAB-MMT during the adsorption. The values of ΔS° were negative depicting the occurrence of some structural changes on the adsorbent surface during the adsorption. The magnitudes of ΔH° and ΔG° for RB, CV, and MB adsorption on BPS-CTAB-MMT were lesser than 20 kJ/mol indicating the removal process was physical in nature (Bouraada et al., 2008). The ΔS° values were negative, while ΔH° values were positive during the study. This means that the negative ΔS° values have a strong influence on the ΔG° values (Cotteta et al., 2014).

5. Desorption studies

The desorption studies aid to enlighten the behavior of adsorption, the restoration of RB, MB, CV from aqueous solutions, recovering of the BPS-CTAB-MMT and its possible employments. The recovery of RB was maximum (42.1%) with 0.1 M NaOH followed by C_2H_5OH (31.2%) > CH_3OH (31.1%) > CH_3OCH_3 (18.1%) (Fig. 4a). A traceable amount of RB was recovered with other tested eluents. The recovery of CV from BPS-CTAB-MMT was maximum (41.9%) with CH_3OCH_3 followed by CH_3OH (34.4%) > C_2H_5OH (29.9%) > CH_3COOH (16.6%) (Fig. 4b). Traces of CV were recovered with other studied eluents. Trace amounts of MB were recovered from BPS-CTAB-MMT by tested eluents (Fig. 4c).

6. Conclusions

In conclusion, CTAB intercalation and BPS functionalization of MMT to develop CTAB-BPS-MMT nano-composite was carried out. The developed composite was mesoporous, thermally stable with only 11% weight loss in temperature range: 25–800 °C, and had a crystallite size of 66 nm. Morphological analysis showed the appearance of large number of non-uniform shaped small particles with few bigger particles along with some sharp edge particles synonymous with rod and crystal shape on CTAB-BPS-MMT. Elemental analysis showed an increase in carbon and bromine content after intercalation and functionalization hinting towards successful formation of CTAB-BPS-MMT. The adsorption of dyes was pH dependent. Kinetics studies indicated the equilibration time of dyes adsorption for specified C_o range: 50–150 mg/L in between 300 and 360 min. The dyes adsorption was endothermic, fitted to Sips isotherm and PSO kinetic models. 42.1 and 41.9% RB and CV dyes were recovered with 0.1 M NaOH and CH_3COCH_3, respectively.

Acknowledgement

The authors would like to extend their sincere appreciation to the Deanship of Scientific Research at King Saud University for funding this work through Research Group No. RG-1437-031.The authors extend their appreciation to Polymer Research Group, Department of Chemistry, Faculty of Science, Tanta University, Tanta, Egypt, for supporting this project.

Appendix A. Supplementary data

Supplementary data related to this article can be found at http://dx.doi.org/10.1016/j.jenvman.2018.04.121.

References

Ahmad, A., Mohd-Setapar, S.H., Chuong, C.S., Khatoon, A., Wani, W.A., Kumar, R., Rafatullah, M., 2015. Recent advances in new generation dye removal technologies: novel search for approaches to reprocess wastewater. RSC Adv. 5, 30801–30818.
Bazin, I., Hassin, A.I.H., Hamouda, Y.H., Mnif, W., Bartegi, A., Lopez-Ferber, M., De Waard, M., Gonzalez, C., 2012. Estrogenic and anti-estrogenic activity of 23 commercial textile dyes. Ecotoxicol. Environ. Saf. 85, 131–136.
Bouraada, M., Lafjah, M., Ouali, M.S., de Menorval, L.C., 2008. Basic dye removal from aqueous solutions by dodecylsulfate- and dodecyl benzene sulfonate-intercalated hydrotalcite. J. Hazard. Mater. 153, 911–918.
Chen, D., Chen, J., Luan, X., Ji, H., Xia, Z., 2011. Characterization of anion–cationic surfactants modified montmorillonite and its application for the removal of methyl orange. Chem. Eng. J. 171, 1150–1158.
Cotteta, L., Almeida, C.A.P., Naidek, N., Viante, M.F., Lopes, M.C., Debacher, N.A., 2014. Adsorption characteristics of montmorillonite clay modified with iron oxide with respect to methylene blue in aqueous media. Appl. Clay Sci. 95, 25–31.
Fan, H., Zhou, L., Jiang, X., Huang, Q., Lang, W., 2014. Adsorption of Cu2+ and

methylene blue on dodecyl sulfobetaine surfactant-modified montmorillonite. Appl. Clay Sci. 5, 150–158.
Forgacs, E., Cserhati, T., Oros, G., 2004. Removal of synthetic dyes from wastewaters: a review. Environ. Inter. 30, 953–971.
Hassanien, M.M., Abou-El-Sherbini, K.S., Al-Muaikel, N.S., 2010. Immobilization of methylene blue onto bentonite and its application in the extraction of mercury (II). J. Hazard. Mater. 178, 94–100.
Khan, M.A., Rao, R.A.K., Ajmal, M., 2008. Heavy Metal pollution and its control through Non-conventional adsorbents (1998-2007): a review. J. Inter. Environ. Appl. Sci. 3 (2), 101–141.
Khan, M.A., Ali, M.S., Alothman, Z.A., Siddiqui, M.R., Al-Lohedan, H.A., 2017. Dodecyl sulfate chain-anchored mercerized lignocellulose agro-waste: an effective and sustainable adsorbent to sequester heavy metal ions from an aqueous phase. Environ. Prog. Sust. Ener. 36, 1676–1684.
Kaniappan, K., Latha, S., 2011. Certain investigations on the formulation and characterization of polystyrene, poly (methyl methacrylate) blends. Inter. J. Chem. Tech. Res. 3, 708–717.
Kumar, B.S., Dhakshinamoorthy, A., Pitchumani, K., 2014. K10 montmorillonite clays as environmentally benign catalysts for organic reactions. Catal. Sci. Technol. 4, 2397–2411.
Liang, Y., Li, H., 2017. A comparison of trimeric surfactant intercalated montmorillonite with its gemini modified one: characterization and application in methyl orange removal. J. Mol. Liq. 227, 139–146.
Liu, B., Wang, X., Yang, B., Sun, R., 2011. Rapid modification of montmorillonite with novel cationic Gemini surfactants and its adsorption for methyl orange. Mater. Chem. Phys. 130, 1220–1226.
Santoso, S.P., Laysandra, L., Putro, J.N., Lie, J., Soetaredjo, F.E., Ismadji, S., Ayucitra, A., Ju, Y.H., 2017. Preparation of nanocrystalline cellulose-montmorillonite composite via thermal radiation for liquid-phase adsorption. J. Mol. Liq. 233, 29–37.
Sarma, G.K., Gupta, S.S., Bhattacharyya, K.G., 2016. Adsorption of crystal violet on raw and acid-treated montmorillonite, K10, in aqueous suspension. J. Environ. Manag. 171, 1–10.
Siboni, M.S., Khataee, A., Hassani, A., Karaca, S., 2015. Preparation, characterization and application of a CTAB-modified nanoclay for the adsorption of an herbicide from aqueous solutions: kinetic and equilibrium studies. Comp. Ren. Chim. 18, 204–214.
Silva, M.M.F., Oliveira, M.M., Avelino, M.C.M., Fonseca, G., Filho, E.C.S., 2012. Adsorption of an industrial anionic dye by modified-KSF-montmorillonite: evaluation of the kinetic, thermodynamic and equilibrium data. Chem. Eng. J. 203, 259–268.
Tangaraj, V., Janot, J.M., Jaber, M., Bechelany, M., Balme, S., 2017. Adsorption and photophysical properties of fluorescent dyes over montmorillonite and saponite modified by surfactant. Chemosphere 184, 1355–1361.
Tong, D.S., Zhou, C.H., Lu, Y., Yu, H., Yu, W.H., 2010. Adsorption of acid red G dye on octadecyltrimethylammoniummontmorillonite. Appl. Clay Sci. 50, 427–431.
Wang, X.S., Zhang, W., 2011. Removal of basic dye crystal violet from aqueous solution by Cu(II)-Loaded montmorillonite. Sep. Sci. Technol. 46, 656–663.
Wang, L., Wang, A., 2008. Adsorption properties of Congo Red from aqueous solution onto surfactant-modified montmorillonite. J. Hazard. Mater. 160, 173–180.
Xue, W., He, H., Zhu, J., Yuan, P., 2007. FTIR investigation of CTAB–Al–montmorillonite complexes. Spectrochim. Part A Mol. Biomol. Spectrosc. 67, 1030–1036.
Yusuf, M., Elfghi, F.M., Zaidi, S.A., Abdullah, E.C., Khan, M.A., 2015. Applications of graphene and its derivatives as an adsorbent for heavy metals and dyes removal: a systematic and comprehensive overview. RSC Adv. 5, 50392–50420.
Yusuf, M., Khan, M.A., Otero, M., Abdullah, E.C., Hosomi, M., Terada, A., Riya, S., 2017. Synthesis of CTAB intercalated graphene and its application for the adsorption of AR265 and AO7 dyes from water. J. Colloid Interf. Sci. 493, 51–61.